In Situ Analysis of the Defect Texture in Liquid Crystal Polymer Solutions under Shear

Lynn M. Walker,† William A. Kernick III, and Norman J. Wagner*

Colburn Laboratory, Department of Chemical Engineering, University of Delaware, Newark, Delaware 19716

Received April 19, 1996; Revised Manuscript Received August 15, 1996[⊗]

ABSTRACT: A combination of two *in situ* small-angle scattering techniques are employed to compare the texture and molecular order in flowing LCPs that exhibit constant viscosities (region II) and shear thinning (region I) at low shear rates. The microstructure is characterized by an overall molecular orientation S_{eff}, a texture correlation length a_c, and an aspect ratio a_r. Results indicate that in region I the texture has a high density of defects and a low overall molecular order, with shear primarily acting to distort the texture. In region II the texture is distorted in the shear direction and the overall molecular orientation is higher, while the primary influence of shear is to refine texture size. The critical Ericksen stress balance is also tested experimentally.

1. Introduction

At low shear rates liquid crystal polymers (LCPs) exhibit a complex supramolecular microstructure, or texture, that is sensitive to shear deformation. This texture consists of a network of defects that disrupt the nematic LCP fluid. The texture directly contributes to the macroscopic flow properties of the material, resulting in a viscoelastic response that may be shear thinning (region I) or constant (region II) at low shear rates,[1] depending on the strength of this texture relative to the applied flow and the mechanical properties of the nematic LCP. The ability to predict the rheology, degree of molecular orientation, and the structure of the defect texture is necessary for the design of processes to produce LCP-based products. At the present time, we lack both an understanding of the nature of the defect texture existing at low shear rates and the quantitative link between this texture and the macroscopic properties.[2]

Combined morphological and rheological studies have elucidated much about the nature of the interaction between deformation and texture. Careful microscopy studies on shearing LCP solutions demonstrated the complex transitions and instabilities exhibited by polymer nematics.[3,4] One key finding is that director tumbling leads to the formation of a textured fluid with multiple levels of microstructure: locally nematic fluid with macroscopic gradients in director orientation that can be both spatially and time varying. Optical measurements demonstrate that shearing at moderate rates will generate a textured microstructure, even when starting with a uniform, aligned nematic fluid.[5] In region II, it appears that a balance exists between the stresses due to shear ($\eta\dot{\gamma}$) and the elastic stresses generated by distortion of the defect texture (K/a^2).[6−8] This balance has been reexpressed as an Ericksen number ($Er = \eta\dot{\gamma}/(K/a^2)$), with the concept of a critical Er suggested for LCPs at low shear rates.[8] Characterizing the texture with a single length scale and elastic constant K may seem a drastic oversimplification, but the incorporation of a single microstructural length scale is capable of explaining the observation of strain-dependent, rather than time-dependent, transient behavior in many of these systems.[9] This assumption of balancing macroscopic and microstructural stresses can only be verified with direct *in situ* measurements of textural properties.

Rheological measurements on concentrated lyotropic and thermotropic LCPs further suggest that the defect texture can influence the rheological behavior in a manner beyond simply providing an "anchor" or obstacle for the flowing nematic fluid.[10] Region I has been associated with a very dense texture that is so defect ridden as to deviate from the scaling mentioned above.[11] This situation is one in which the distortion of the defects is thought to directly contribute to the bulk viscosity.

Previous studies using *in situ* probes to study defect texture have characterized the change in the average overall molecular order with increasing shear. At rest, the defect texture leads to a nematic fluid with no net molecular orientation, often envisioned as a polydomain microstructure, despite the relatively high degree of molecular order present in the pure nematic fluid. Under shear the distribution of molecular orientations is distorted toward the shear direction; hence, a measure of this distortion probes the influence of shear on the texture. Different techniques have been employed to measure molecular order: birefringence,[12,13] SAXS,[14,15] and SANS.[16−18] Recently, the equivalence and discrepancies between these different techniques has been examined.[19] At this time, the relationship between scattering patterns and molecular orientation is well-founded, but a definitive link between rheology, molecular orientation, and defect texture has not been made. Significant steps have been taken in this direction through the development of a polydomain model[9] based on the critical Ericksen number concept.[8]

Small-angle light scattering probes large length scales, comparable to the wavelength of light. Given the optical activity of flowing LCPs,[20,21] this is the length scale on which the texture has a strong influence. Consequently, SALS[22−24] and dichroism[25,26] have been used to probe the defect texture in flowing LCP systems. However, much of this work has been involved with either developing the technique or probing structures observed at high shear rates, rather than quantifying the changes in defect texture accompanying region I rheology.

* Corresponding author: wagner@che.udel.edu.
† Present address: Department of Chemical Engineering, Katholieke Universiteit Leuven, de Croylaan 46, Leuven, Belgium B-3001.
⊗ Abstract published in *Advance ACS Abstracts,* January 15, 1997.

S0024-9297(96)00590-6 CCC: $14.00

In this work, we employ two scattering techniques to characterize both the texture and molecular orientation. Flow small-angle neutron scattering (SANS) probes the overall orientation of the LCP molecules, as characterized by an effective order parameter S_{eff}, without significant scattering from the defects themselves. Small-angle light scattering (F-SALS) uses polarized light to probe micron length scales characteristic of the defect texture. This latter technique is performed *in situ* with rheological measurements in a specially constructed apparatus. Without making specific assumptions about the structure of the defects, we use F-SALS to determine an average texture correlation length a_c and an aspect ratio characterizing the deformation of the defect texture a_r. The influence of shear on these three parameters S_{eff}, a_c, and a_r is probed and compared to the macroscopic rheological behavior. The study is restricted to the behavior of model lyotropic systems at low shear rates, where all three properties are thought to be important. Specifically, the variation of the molecular and defect microstructures (as characterized by S_{eff}, a_c, and a_r) are studied in regions I and II for systems that have been investigated in previous rheological studies.[4,10,11,27]

2. Materials and Methods

Two different lyotropic LCP systems are studied in this work: hydroxypropyl cellulose (HPC) and poly(γ-benzyl L-glutamate) (PBLG). Deuterated solvents are used for the SANS studies to avoid the large incoherent scattering from hydrogen and to provide necessary contrast. Five solutions of PBLG are investigated, two with SANS and three with F-SALS. For SANS, PBLG (MW 235 000) is dissolved in dry, deuterated dimethylformamide (d-DMF) at concentrations of 17 and 30 wt %. Difficulties involved in working with this solvent and the special procedures required are discussed in an earlier publication.[28] For F-SALS studies, solutions of 25, 37, and 40 wt % PBLG (MW 238 000) are prepared in *m*-cresol. The density of d-DMF is nearly equivalent to that of *m*-cresol (ρ = 1.03 g/mL), but the viscosity is lower by a factor of 5. Based on the equivalence of the densities, we expect the phase behavior in the two different solvents to be comparable when cast in terms of weight percent polymer. The difference in solvent viscosity results in an inversely proportional change in the rotational diffusivity of the director. The rheological behavior of the nematic fluid should depend on shear rates scaled with the rotational diffusivity; therefore, we assume that the rheological transitions associated with the nematic fluid are shifted to higher shear rates by a factor of 5 in d-DMF.[16] However, we do caution that specific solvent effects may influence this equivalence.[17,29,30]

A 57 wt % HPC-E (Klucel E from Aqualon) in D_2O solution is prepared by weight for the SANS study while a corresponding 60 wt % HPC-E in water solution is prepared for F-SALS. Based on the density difference of the solvents, the concentration of the sample in deuterated solvent is adjusted so the two solutions are of equivalent volume fraction. The phase behavior of similar solutions has been recently studied,[31] indicating that 60 wt % solutions at 25 °C may be biphasic. However, this result depends strongly on the specific polymer sample under investigation; optical microscopy of our samples showed no signs of isotropic droplets or biphasic behavior, indicating a homogeneous liquid crystal phase.

Three classes of behavior are distinguishable from the rheological studies. Nematic solutions below 20 wt % PBLG exhibit a viscoelastic response considered prototypical of a nematic solution of stiff rods.[32] Solutions from about 20 wt % up to 37 wt % PBLG exhibit a plateau viscosity (region II) that increases with increasing concentration,[10,27,33,34] distinguishing them from these prototypical nematic solutions. At higher concentrations of PBLG, and equivalently for high concentrations of HPC (e.g., 60 wt % HPC-E/water and 57 wt % HPC-E/D_2O), region I rheology is observed, a behavior generally associated with a highly defect-ridden texture.[10,11,27] The critical shear rates for the transition from region I to region II are approximately 0.3 and 0.4 s^{-1} for the 40 wt % PBLG and 60 wt % HPC-E solutions, respectively.

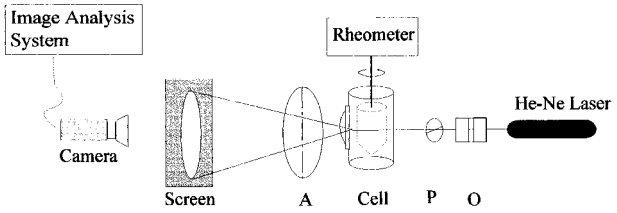

Figure 1. Schematic diagram of the F-SALS apparatus. The beam passes first through a pinhole and filter (O) and then a polarizing prism (A) before impinging on the shear cell. The scattered beam is polarized (P) and then is projected onto a vellum screen before capture.

2.1. F-SANS. Flow SANS studies are performed on the 30 m NG3 beamline at the National Institute of Standards and Technology in Gaithersburg, MD. A quartz Couette cell with a fixed stator and rotating outer cup is used to provide a controlled shear field across a 0.25 mm gap. The cell is enclosed in a nitrogen environment to prevent contamination of the d-DMF with water and to limit solvent evaporation. The neutron beam passes through the center of the cell, providing a projection of the flow−vorticity scattering plane. Standard techniques are used to reduce the measured neutron intensities to an absolute scale and remove instrument effects.[35]

2.2. F-SALS Device. Flow small-angle light scattering (F-SALS) studies are performed on a unique rheooptic device developed and built in our laboratory. Figure 1 shows a schematic diagram of the F-SALS device. The flow field is controlled and measured with a Bohlin CS-50 rheometer, a controlled stress device. The flow cell is a glass Couette cell (DIN C-14) that has a rotating bob and a gap of 1 mm. F-SALS experiments are performed by passing a beam of polarized He−Ne (λ = 6328 Å) laser light through the diameter of the Couette cell, orthogonal to the rotation axis of the bob. This provides scattering patterns that are a projection of the flow−vorticity (1−3) plane. A neutral-density filter and pinhole (O in the figure) are included in the optical train to control the incident beam intensity. The incident beam is polarized using a Glan-Thompson calcite prism (P) while a 45.4 mm diameter sheet polarizer (A) acts as the analyzer. The laser is randomly polarized and both the prism and polarizing sheet are adjustable or removable so that a variety of polarization states can be studied. In the bulk of this work, polarizers are set such that the incident beam is polarized in the flow direction (H) while the analyzer is rotated by 90° to align with the vorticity direction (V). Multiple scattering from the cell is minimal as it is polished, high-quality optical quartz. The full q range available, with $q \equiv (4\pi/\lambda)\sin(\theta/2)$, from this instrument is roughly 3500−35000 cm^{-1} ($2° < \theta < 20°$), although in this study only angles below $\theta \approx 12°$ are probed. Scattered patterns are projected onto a vellum screen with a small beamstop to block the main beam. The patterns are captured with a $^1/_2$-in. black and white CCD video camera and digitized with a MATROX frame grabber. During live capture, four images are averaged together over $\approx^1/_6$th of a second to create a pattern for analysis.

In the Couette geometry, the sample is crossed twice by the beam, so that part of the incident intensity is scattered during the first traversal of the Couette cell. A concern involved with this geometry is the cylindrical glass−air interface through which the scattered light must exit. To correct for these effects, a combination of corrective lenses are attached to the outer surface of the cell. As the beam is scattered from the second scattering volume, it exits the cylindrical cell into a cylindrical lens fitted to the cell with a thin film of refractive index matching fluid. The scattered light then enters a partial spherical lens matted to the flat side of this cylindrical lens. These lenses are designed such that the scattered light from the second traversal through the sample exits perpendicularly through the glass−air interface, thus avoiding refraction. This

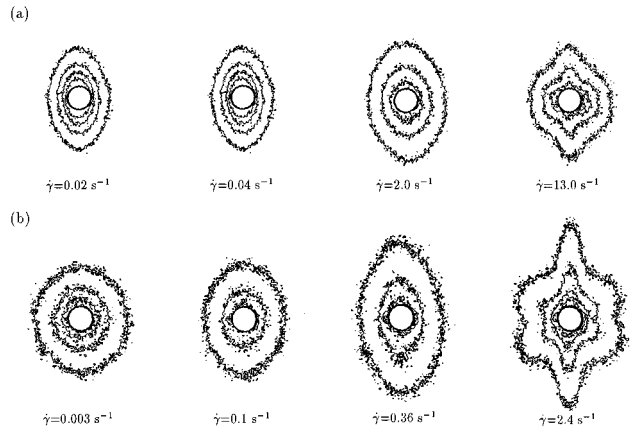

Figure 2. Depolarized (H_V) F-SALS patterns from LCP solutions under shear: (a) 37 wt % PBLG/*m*-cresol and (b) 60 wt % HPC-E/water. The flow direction is horizontal and the shear rates span regions I, II, and III.

is important to ensure both the geometric accuracy and the proper intensity of the pattern on the detector. Calibration of the scattering cell and assessment of accuracy were performed by scattering from a solution of monodisperse latex spheres ($d = 2.875 \pm 0.133$ μm, Polybead cat. no. 17134) in water.[36]

3. Scattering Analysis

3.1. F-SANS Analysis: Determination of S_{eff}. The measured two-dimensional SANS scattering patterns provide considerable information about the shear-induced structure. To extract quantitative information about the degree of molecular alignment, we developed a molecular scattering model[28] to measure molecular order parameters by fitting to experimentally measured patterns. In a later work,[16] we employed this molecular model to demonstrate that an overall uniaxial order parameter can be directly extracted from the anisotropy of the scattering pattern via a weighted averaging of the measured scattering intensity $I(q,\phi)$. The anisotropy in the azimuthal angle is captured by defining an "alignment factor" or $A_f(q)$:

$$A_f(q) = \frac{\int_0^{2\pi} I(q,\phi) \cos(2\phi)\, d\phi}{\int_0^{2\pi} I(q,\phi)\, d\phi} \qquad (1)$$

with $\phi = 0$ defined in the shear direction. For the range of scattering vector (q) available in SANS, the alignment factor is constant and ranges from 0 for an isotropic scattering to -1 for a perfectly aligned sample. As this has been shown to be a direct measure of the macroscopic order parameter in the case of uniaxially aligned rigid rods,[28] we define the effective order parameter $S_{eff} = -A_f^{\infty}$, defined as $A_f(q \to \infty)$. Note that in this experimental geometry, $S_{eff} = S_{11} - S_{33}$ where 1 is the flow and 3 the vorticity direction, where S_{ii} are components of a second-order tensor characterizing the order.[32]

3.2. F-SALS Analysis: Determination of a_c and a_r. Depolarized SALS patterns obtained on flowing LCPs are more complex than those obtaned by SANS.[22] Figure 2 shows contour plots of F-SALS patterns for both 60 wt % HPC-E/water and 37 wt % PBLG/*m*-cresol as functions of increasing shear rate. Three types of patterns are observed, each corresponding to a different rheological behavior: circular patterns, elliptical patterns with the long axis perpendicular to flow, and superpositions of a four-lobed pattern with a vertical flare. The nearly circular patterns, which suggest an isotropic defect texture, are seen only at low shear rates in materials that exhibit region I rheology. These patterns distort elliptically as shear rates increase into region II, indicating a preferential stretching of the texture in the shear direction (alignment in the flow direction leads to increased scattering intensity orthogonal, or 90°, to the flow direction). Finally, the complex patterns with lobes and a vertical streak appear in all solutions at higher shear rates, due to scattering from a more specific feature of the defect texture. The two latter behaviors have been reported previously for both PBLG/*m*-cresol and HPC/water solutions.[22] The anisotropy in the depolarized scattering also leads to a linear dichroism, as previously reported for PBLG/*m*-cresol.[37] The intensity streak in the vorticity direction has been attributed to scattering from defect lines oriented in the flow direction.[24] The appearance of this streak corresponds to a distinct change in the shape of the $I_{H_V}(q)$ curve in the vertical direction, which can be fit to the form factor of a rod.[36] In this work, patterns exhibiting this streak will not be analyzed.

These F-SALS patterns indicate a complicated structure (defect texture) convoluted with a complicated scattering mechanism (depolarization). A complete analysis of the two-dimensional scattering from an optically active material with an evolving defect texture has not yet been achieved, due primarily to a lack of knowledge of the microstructure. Thus, direct inversion of the scattering patterns back to a real space structure is an ill-posed problem. However, considerable quantitative information characteristic of the defect texture can be directly extracted from the scattering patterns without detailed molecular models. The characteristic texture size can be extracted from the q dependence of the intensity while the distortion of the texture can be determined from the anisotropy of the patterns.

To extract the characteristic texture size, we extend a classic scattering model developed to account for the scattering of radiation by an inhomogeneous solid. This technique, developed by Debye and Bueche,[38] was intended to determine the length scale of density fluctuations in solid materials measured by X-ray or polarized light scattering. The authors argued that in a random inhomogeneous material, in which regions of constant density are separated by sharp boundaries, the correlation function of the density $g_\rho(r)$ of the material may be given by a simple exponential decay. Using this exponential dependence, the scattered intensity is determined via Fourier transform.[39] The exponential decay length is interpreted to be the characteristic length scale of the density fluctuations (domain size).[40]

To extend this model to depolarized scattering from the defect-ridden nematic fluid, we consider fluctuations in polarizability rather than density fluctuations. Our concern is with depolarized scattering from fluctuations in the orientation of the local nematic fluid between the defects. In the nematic fluid, the local orientation of the nematic sets the local polarizability, which is very anisotropic. Defects that disrupt the nematic fluid create spatial gradients in the polarizability that results in the observed depolarized scattering, as has been observed in other, microstructured polymer systems.[41] The spatial correlation function of the director orientations is then approximated by

$$g_n(r) \approx \exp(-r/a_c) \qquad (2)$$

That is, the orientation correlations of the polarizability

tensor decay exponentially with distance in the sample. As the decorrelation is due to the presence of defects, the length scale a_c characterizes the average defect density (a pure nematic fluid would have $a_c \rightarrow \infty$).

As in the original work,[38] a Fourier transform of this distribution function yields an expression for the depolarized scattering intensity

$$I_{H_V}(q) = \frac{I_0 a_c^3}{\{1 + (qa_c)^2\}^2} \tag{3}$$

where I_0 is a collection of instrument and material constants. Thus, we propose eq 3 as a method to determine the correlation length of the defect texture. Plots of $I_{H_V}^{-1/2}(q)$ versus q^2 should yield straight lines such that

$$\text{slope} = \frac{a_c^2}{(I_0 a_c^3)^{1/2}}$$

$$\text{intercept} = \frac{1}{(I_0 a_c^3)^{1/2}} \tag{4}$$

Experimentally, the correlation length a_c is determined from the ratio of slope to intercept (a_c^2 = slope/intercept) of the circularly averaged Debye−Bueche plots of our F-SALS patterns. We note that recent work on block copolymer systems[41] proposes a similar result, and this is based on much earlier results from the literature.[42]

In interpreting the F-SALS patterns, we directly identify this correlation length with the texture size a used in the macroscopic stress balance and polydomain models. Indeed, in the rheological models, the texture size occurs because the spatial distortion of the director field gives rise to elasticity (Frank elasticity). Thus, the texture size important in the critical *Er* number concept is a mechanical measure of the length scale over which the director orientation is correlated. The optical length defined above has the same physical interpretation, and so the two should be essentially identical. What differs, however, is the identification of the characteristic lengths with the size of a "domain", which is an artificial construct used to pictorially represent the defect texture. Indeed, only if the director orientation is completely decoupled between domains (i.e., the director orientation acts like a random walk) will these correlation lengths equal the "domain" size. More realistically, we expect that the director orientation to be correlated over multiple "domains" if the domain size becomes limited by the minimum allowed bending of the director. Given our present understanding of the texture, it may be more prudent to abandon the simplified domain picture and simply recognize that the optical and mechanical correlation lengths should be comparable.

The analysis is performed by averaging around the two-dimensional $I_{H_V}(q,\phi)$ pixel maps, thereby removing the dependence on the azimuthal angle. An example of these Debye−Bueche plots is shown in Figure 3 for 37 wt % PBLG/*m*-cresol. As the shear rate increases, the slope of the linear fit decreases without appreciable change in the intercept, indicating that the correlation length is decreasing. I_0 is related to instrument and material factors and it should not vary with shear rate. To be consistent in the fitting routine, the range of data used to determine a_c was chosen such that I_0 remains constant for a given sample.

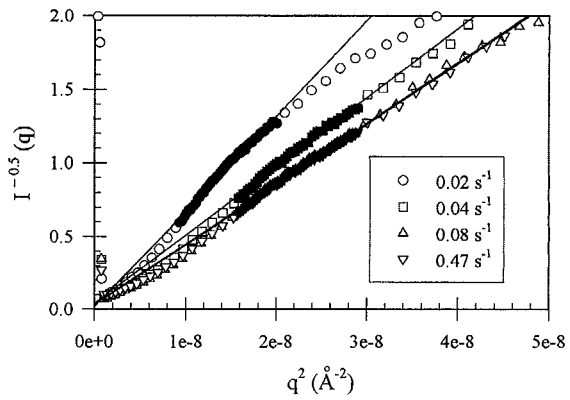

Figure 3. Debye−Bueche plots for the F-SALS patterns from a 37 wt % PBLG/*m*-cresol solution. Symbols indicate the measured intensity while the lines are the linear fits to the data.

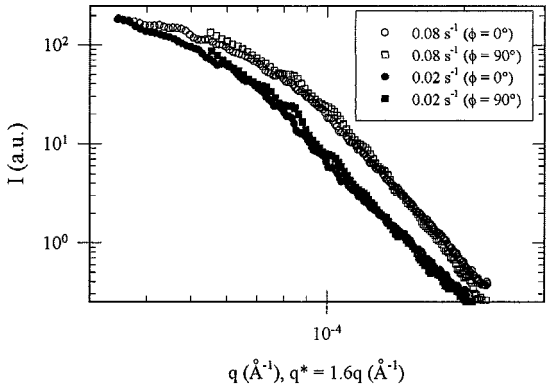

Figure 4. Vertical (vorticity direction) scattering intensity and shifted horizontal (flow direction) scattering intensity of 37 wt % PBLG/*m*-cresol at two different shear rates. In both cases, $a_r = 1.6$.

The distortion of the patterns from circular to elliptical indicates that shear acts to stretch the defect texture in the flow direction. To characterize this distortion, the aspect ratio of the F-SALS patterns is determined as follows: for a given intensity $I^*_{H_V}$, the corresponding q value in each of the horizontal and vertical directions is determined. The aspect ratio is simply defined as

$$a_r = q^*_V/q^*_H \tag{5}$$

The aspect ratio is found to be independent of scattering angle (q) for most of the measurable range. Figure 4 demonstrates this for the 37 wt % PBLG/*m*-cresol patterns. In the figure, the vertical intensity is shown on the measured q axis while the horizontal scattering is shifted by a factor of 1.6; this value of $a_r = 1.6$ was found for all shear rates in region II for this solution.

With depolarized light scattering, stray scattering from the cell and multiple scattering from the sample must be considered. The samples probed here have a high transmission and the depolarized scattering from the cell itself is minimal. Therefore, we expect the measured patterns reflect primarily single scattered light. Indeed, the shear-induced anisotropy of the patterns would not be a consequence of multiple scattering processes, which would lead to an isotropic pattern. We cannot quantitatively correct for the influence of the multiple scattering on our measurements at present, but the presence of an additional, isotropic background would lead to our underestimation of the shear-induced alignment in the sample. Further, the primary effects on the analysis of the Debye−Bueche

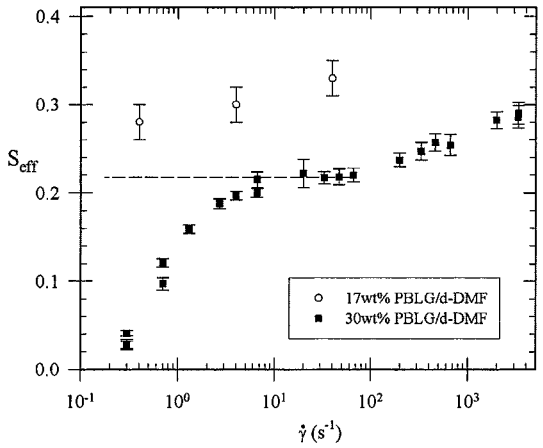

Figure 5. Overall molecular order characterized by S_{eff} of 17 wt % PBLG and 30 wt % PBLG in d-DMF as a function of shear rate.

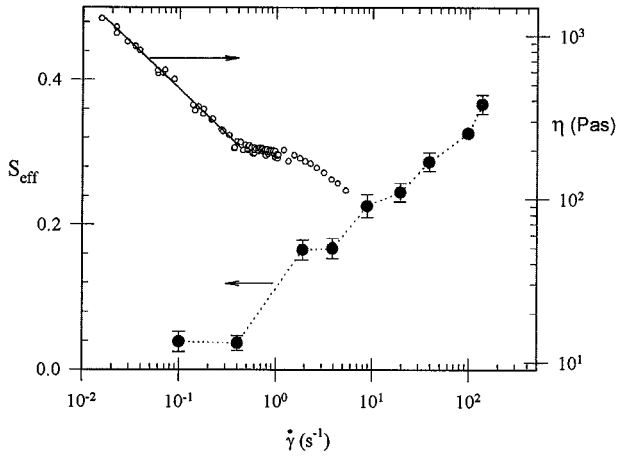

Figure 6. Overall molecular order parameter S_{eff} for the system 57 wt % HPC-E/D_2O as a function of shear rate.

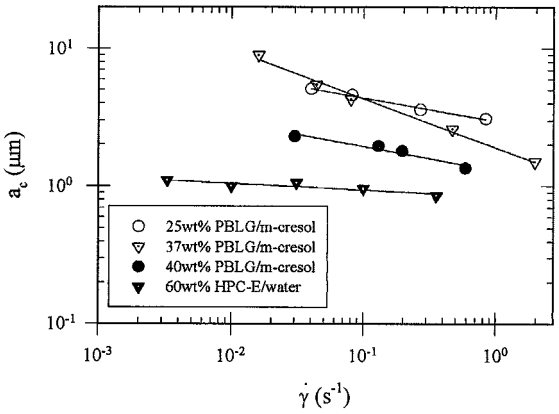

Figure 7. Correlation lengths a_c determined from F-SALS patterns for solutions that exhibit region I (filled) at low shear rates and those that exhibit only region II (open) at low shear rates.

plots would be (i) to increase I_0, which would not lead to any change in the determination of the correlation length as it is independent of this, and (ii) to add a background scattering. The latter would lead to a negative deviation from the Debye−Bueche fits, as observed in Figure 3.

4. Results

4.1. F-SANS Results (S_{eff}). At rest, the F-SANS patterns are observed to be isotropic for all the solutions studied ($S_{eff} = 0$), demonstrating the ability of the defect texture to disorder the fluid at a macroscopic level. The local molecular order is expected to be approximately 0.8 as measured by NMR.[43] At rest, the sample is composed of randomly oriented "domains" much smaller than the thickness of the sample. This results in zero net overall molecular alignment as probed by SANS. Under shear, the patterns become anisotropic, elongated perpendicular to the flow direction, as previously published.[16]

Values for S_{eff} calculated from eq 1 are reported for both the 17 wt % and 30 wt % PBLG solutions in Figure 5. The less concentrated of the two shows a weak dependence on shear rate, while the 30 wt % solution shows a strong and nonlinear dependence on shear rate. Previous measurements of molecular orientation in PBG solutions using birefringence[12] and more recently SANS[19] show that nematic solutions of 20 wt % PBLG and below have nearly constant orientation in region II, consistent with our results for the 17 wt % solution. No comparative studies have been performed on solutions at concentrations higher than 20 wt % PBLG. The dependence of net molecular alignment on shear rate for the 30 wt % sample suggests a strong coupling between texture and shear. Note that the solutions have a constant viscosity in this range of shear. However, for the 30 wt % solution the plateau viscosity is increasing with concentration, a factor that has already been attributed to stronger textural influence.[33,44]

Results for the 57 wt % HPC-E/D_2O solution are shown in Figure 6. Clearly, shear increases the overall molecular order in regions II and III. For low shear rates, associated with region I rheology, the molecular order is almost zero and independent of shear rate. These results agree with SAXS,[15] SANS,[18] and birefringence[45] results for similar HPC solutions.

4.2. F-SALS Results (a_c and a_r). The correlation lengths a_c measured for four different LCP solutions are shown in Figure 7. For the 25 and 37 wt % PBLG/*m*-cresol solutions, the correlation length, which we relate directly to the texture size, is seen to decrease as shear rate increases. The slopes of these lines are −0.2 and −0.4, neither of which adheres to the simple scaling suggested by balancing stresses; $a \propto \dot{\gamma}^{-1/2}$.[8,9] The magnitude of the measured texture size is in agreement with that measured during and directly after flow using microscopy.[4]

For the two solutions which exhibit region I, 40 wt % PBLG/d-DMF and 60 wt % HPC-E/water, the correlation length is smaller and, in the case of HPC, less dependent on shear rate. The smaller size indicates a significantly higher density of defects in these concentrated solutions.

The aspect ratios a_r are shown in Figure 8 as a function of applied shear. In region II the a_r is 1.7 for a 25 wt % PBLG solution and 1.6 for a 37 wt % PBLG solution, corresponding to a distortion of as much as 70% in the shear direction. The level of distortion is shear rate independent in region II and decreases with increasing concentration. With decreasing shear rates in region I (Figure 8), the a_r limits toward a value of 1 (circular pattern). These patterns approach the distortion seen in the less concentrated materials at the highest shear rates shown (above these shear rates the appearance of the vertical streak and lobes limits our analysis).

5. Discussion

The influence of concentration and shear rate on both net molecular orientation and texture alignment as well

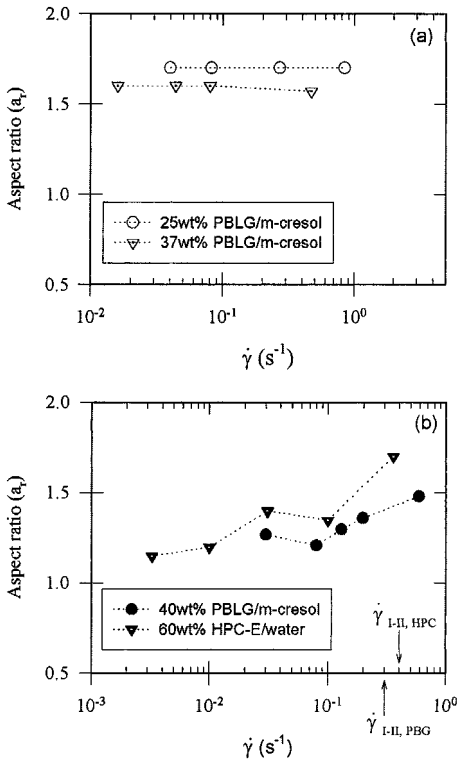

Figure 8. Aspect ratios a_r extracted from F-SALS patterns: (a) region II materials; (b) region I materials.

as texture size is probed for two model LCP solutions. Region II in PBLG solutions, which is thought to be reasonably well understood, shows two different types of behavior depending on concentration. Above the point of complete anisotropy ($c_a \approx 12$ wt %), the plateau viscosity decreases with increasing concentration, but then begins to increase again above concentrations of about 20 wt %. By comparing our results with other microstructural studies performed on PBG, it is possible to identify this behavior with an increase of the relative contribution of the defect texture to the stress as concentration increases. At concentrations just above c_a, there is qualitative agreement between rheological data and a polydomain model which couples the texture to the macroscopic behavior.[9] The model assumes the validity of the Ericksen stress balance and that the net molecular alignment is independent of shear rate, in other words, that the primary influence of the shear is to induce texture refinement with a single textural length scale.

For low-concentration nematics (12−20 wt %), the molecular order has been probed via birefringence[12] SAXS,[19] and SANS[19] in region II. Results indicate a shear-rate-independent S_{eff} which increases with increasing concentration, in agreement with molecular theory.[46] Our SANS results at 17 wt % PBLG/d-DMF concur with these reported findings. Texture size has not been determined via F-SALS in this concentration range as the low shear rates needed to observe elliptical patterns were not probed. However, texture size refinement is observed using polarimetry techniques[47] in this concentration regime, but with an exponent $a \propto \dot{\gamma}^{-0.33}$ that is less than expected from the Ericksen stress balance. It is not clear if the lack of agreement with the simple stress balance is due to extracting a single length scale from such a deformed texture or if there is a more fundamental problem in the expression for the elastic stress.

At higher concentrations of PBLG (above approximately 20 wt %), the viscosity retains a region II plateau, yet qualitative changes in transient rheological behavior have been observed.[10,33] The SANS results for the 30 wt % PBLG indicate that the overall order initially increases with shear rate well into region II and then plateaus followed by a further increase in region III. A measure of the first normal stress difference, which has not been made for this solution, would enable more precisely correlating the changes in S_{eff} with specific behavior of the nematic director. Our SANS results also show that the magnitude of S_{eff} and the texture anisotropy at a given $\dot{\gamma}$ are now decreasing as the concentration increases. This demonstrates that although there is increased molecular alignment due to the increase in concentration, the macroscopic disordering influence of the defect texture becomes dominant. Texture size refinement is still observed with a similar shear rate dependence as measured in earlier studies. The exponent (−0.4) is closer to being in agreement with the Ericksen stress balance (−0.5). Therefore, in this concentration regime (20−37 wt % PBLG), the polydomain model may fail due to the assumption that the molecular and textural order can be decoupled. Our measurements show a shear-dependent net molecular alignment and anisotropy ratio, and a texture size that decreases with shear rate. Consistent with the observed decrease in net molecular order parameter with increase in concentration, these microscopic measurements indicate a change in the relationship between texture and deformation for this intermediate concentration regime.

Region I is observed for 40 wt % PBLG solutions as well as 60 wt % HPC-E/water and 57 wt % HPC-E/D_2O. Rheological studies indicate that the behavior is shear induced and extremely long-lived.[10] The F-SALS study indicates a further reduction in texture size (a_c) between 37 and 40 wt % PBLG and an aspect ratio which is now shear rate dependent. These effects are even clearer for region I in the 60 wt % HPC-E/water system, which shows a smaller texture size that is almost independent of applied shear rate. In the HPC system, the scattering patterns are nearly circular at low shear rates but deform with increasing shear rate. Measurements of S_{eff} demonstrate that, in region I, the net molecular order is very low and not strongly influenced by shear rate. In summary, the defect density in region I is much more dense than in the lower concentration solutions. The strong shear-thinning characteristic of region I is accompanied by increasing shear distortion of the texture without significant overall molecular alignment and only weak texture size refinement. The latter is only roughly following the prediction of the critical Ericksen stress hypothesis. In this regime the polydomain model is thought to fail because the direct contribution to the stress from distortion of the defect network is not included. Although the major rheological characteristics of region I are common to both PBLG and HPC solutions, subtle differences do exist.[10,11] Recent scattering measurements suggest that there may be additional ordering present in concentrated PBLG solutions that could explain some of these differences.[48] Therefore, further work is required to fully understand the complex texture and molecular structure govening region I behavior.

6. Conclusions

In this work, we use a combination of scattering techniques to quantify the influence of shear flow on

the defect texture observed in LCP solutions. Through comparison of our measurements of molecular order (SANS) and texture size and distortion (F-SALS) with rheology, we can now summarize the coupling of microstructure and shear flow as follows. In region I the flow does not induce any net molecular order; rather the very fine texture is being stretched with only a small increase in defect density. This is consistent with the concept that region I rheology reflects the balance between shear stress and direct stresses due to texture distortion.[10] F-SALS indicates that in region II the texture has reached a stationary level of distortion and the primary influence of shear is to reduce the texture size by increasing the density of defects. Concentration alters the relationship between overall molecular order and shear rate; at low to moderate concentrations S_{eff} is relatively large and constant in region II while at higher concentrations the S_{eff} increases from zero at low shear rates with increasing shear rate.

This information should be of use in the development of texture-based models of LCP rheology. Only the low-concentration nematic fluid exhibits qualitatively the same rheological behavior predicted by the polydomain model,[9] and further investigations need to include aspects of defect generation, texture distortion, as well as net or overall molecular alignment on the macroscopic stress. These results suggest that the texture is as strong as the applied flow in region I, leading to texture elasticity dominating the rheology. Lowering the concentration at a fixed shear rate results in a lower defect density and a commensurate loss of region I rheology. In region II, increasing the shear rate creates more defects at roughly constant texture distortion, but with strong flow alignment of the net overall molecular order. Further reduction in concentration results in a fluid with high net molecular order at low shear rates and very little direct influence of the defect texture on the flow. A more detailed knowledge of the defects in LCPs and their mechanical properties would be beneficial in interpreting the experimental measurements presented here.

Acknowledgment. This work was supported under NSF Grant CTS-9158146. This material is based on activities supported by the National Science Foundation under agreement No. DMR-9122444. We acknowledge the support of the National Institute of Standards and Technology, U.S. Department of Commerce, in providing the facilities for the SANS experiments.

References and Notes

(1) Asada, T.; Onogi, S.; Yanase, H. *Polym. Eng. Sci.* **1984**, *24*, 355−360.
(2) Marrucci, G.; Greco, F. *Adv. Chem. Phys.* **1993**, *86*, 331−404.
(3) Larson, R. G.; Mead, D. W. *Liq. Cryst.* **1993**, *15*, 151−169.
(4) Vermant, J.; Moldenaers, P.; Picken, S. J.; Mewis, J. *J. Non-Newtonian Fluid Mech.* **1994**, *53*, 1−23.
(5) Muller, J. A.; Stein, R. S.; Winter, H. H. *Rheol. Acta* **1996**, *35*, 160−167.
(6) Marrucci, G. In *Proceedings of the IX International Congress on Rheology*, 1984, pp 441−448.
(7) Wissbrun, K. F. *Faraday Discuss. Chem. Soc.* **1985**, *79*, 161−173.
(8) Burghardt, W. R.; Fuller, G. G. *J. Rheol.* **1990**, *34*, 959−992.
(9) Larson R. G.; Doi, M. *J. Rheol.* **1991**, *35*, 539−563.
(10) Walker, L. M.; Wagner, N. J.; Larson, R. G.; Mirau, P. A.; Moldenaers, P. *J. Rheol.* **1995**, *39*, 925−952.
(11) Walker, L. M.; Wagner, N. J. *J. Rheol.* **1993**, *38*, 1525−1547.
(12) Hongladarom, K.; Burghardt, W. R.; Baek, S.-G.; Cementwala, S.; Magda, J. J. *Macromolecules* **1993**, *26*, 772−784.
(13) Hongladarom, K.; Burghardt, W. R. *Macromolecules* **1993**, *26*, 785−794.
(14) Picken, S. J.; Aerts, J.; Visser, R.; Northolt, M. G. *Macromolecules* **1990**, *23*, 3849−3854.
(15) Keates, P.; Mitchell, G. R.; Peuvrel-Disdier, E.; Navard, P. *Polymer* **1993**, *34*, 1316−1319.
(16) Walker, L. M.; Wagner, N. J. *Macromolecules* **1996**, *29*, 2298−2301.
(17) Dadmun, M. D.; Han, C. C. *Macromolecules* **1994**, *27*, 7522−7532.
(18) Dadmun, M. D. In *Flow-Induced Structure in Polymers*; ACS Symposium Series 597; American Chemical Society: Washington, DC, 1995; Chapter 22.
(19) Hongladarom, K.; Ugaz, V.; Cinader, D.; Burghardt, W. R.; Quintana, J. P.; Hsiao, B. S.; Dadmun, M. D.; Hamilton, W. A.; Butler, P. D. *Macromolecules* **1996**, *29*, 5346.
(20) Mackley. M. R.; Pinaud, F.; Siekmann, G. *Polymer* **1981**, *22*, 437−446.
(21) De'Nève, T.; Navard, P.; Kléman, M. *J. Rheol.* **1993**, *37*, 515−529.
(22) Takebe, T.; Hashimoto, T.; Ernst, B.; Navard, P.; Stein, R. S. *J. Chem. Phys.* **1990**, *92*, 1386−1396.
(23) Picken, S. J.; Aerts, J.; Doppert, H. L.; Reuvers, A. J.; Northolt, M. G. *Macromolecules* **1991**, *24*, 1366−1375.
(24) Patlazhan, S.; Riti, J. B.; Navard, P. *Macromolecules* **1996**, *29*, 2029.
(25) Burghardt, W. R.; Fuller, G. G. *Macromolecules* **1991**, *24*, 2546−2555.
(26) Moldenaers, P.; Fuller, G.; Mewis, J. *Macromolecules* **1989**, *22*, 960−965.
(27) Larson, R. G.; Promislow, J.; Baek, S.-G.; Magda, J. J. In *Proceedings of an Osaka University Symposium on Ordering in Macromolecular Systems*; Springer-Verlag: Berlin, 1993.
(28) Wagner, N. J.; Walker, L. M. *Macromolecules* **1994**, *27*, 5979−5986.
(29) DuPre, D. B.; Duke, R. W. *J. Chem. Phys.* **1975**, *63*, 143−148.
(30) Sato, T.; Teramoto, A. *Macromolecules* **1996**, *29*, 4107−4114.
(31) Guido, S.; Grizzuti, N. *Rheol. Acta* **1995**, *34*, 137−146.
(32) Doi, M.; Edwards, S. F. *The Theory of Polymer Dynamics*; Clarendon Press: Oxford, 1986.
(33) Walker, L. M.; Mortier, M.; Moldenaers, P. *J. Rheol.* **1996**, *40*, 967−981.
(34) Baek, S.-G.; Magda, J. J.; Larson, R. G. *J. Rheol.* **1993**, *37*, 1201−1224.
(35) Barker, J.; Krueger, S.; Hammouda, B. SANS Data Reduction and Imaging Software. Technical Report, National Institute of Standards and Technology, Cold Neutron Research Facility, 1993.
(36) Walker, L. M. Ph.D. Thesis, University of Delaware, 1995.
(37) Moldenaers, P.; Fuller, G.; Mewis, J. *Macromolecules* **1989**, *22*, 960−965.
(38) Debye P.; Bueche, A. M. *J. Appl. Polym. Sci.* **1949**, *20*, 518−525.
(39) Higgins J.; Benoit, H. C. *Polymers and Neutron Scattering;* Oxford Science: Oxford, 1994.
(40) Stein, R. S. In *Polymer Blends*; Paul, D. R., Newman, S. Eds.; Academic Press: New York, 1978; Vol. 1, p 393.
(41) Garetz, B. A.; Dai, H. J.; Jonnulagadda, S. V.; Balsara, N. P. *Macromolecules* **1993**, *26*, 3151−3155.
(42) Stein, R. S.; Wilson, P. R. *J. App. Phys.* **1962**, *33*, 1914−1921.
(43) Abe, A.; Yamazaki, T. *Macromolecules* **1989**, *22*, 2138−2145.
(44) Larson R. G. *Rheol. Acta* **1996**, *35*, 150−159.
(45) Burghardt, W. R.; Bedford, B.; Hongladarom, K.; Mahoney, M. In *Flow-Induced Structure in Polymers*; ACS Symposium Series 597; American Chemical Society.
(46) Doi, M.; Edwards, S. F. *The Theory of Polymer Dynamics*; International Series of Micrographs on Physics; Oxford Science: Oxford, 1986; Vol. 73.
(47) Burghardt, W. R.; Hongladarom, K. *Macromolecules* **1994**, *27*, 2327−2329.
(48) Burghardt, W. R., private communication.

MA960590E